Recovery of Platinum Group Metals from Acidic Solutions Using Dithio and Benzimidazolylthio Functionalized Resins

Masivuye Momelezi Mahleba * , Jean-Luc Mukaba , Zenixole Richman Tshentu

Posted Date: 30 April 2025

doi: 10.20944/preprints202504.2633.v1

Keywords: Platinum group metals; functionalized Merrifield's resin; adsorption studies

 doi:10.20944/preprints202504.2633.v1

Article

Recovery of Platinum Group Metals from Acidic Solutions Using Dithio and Benzimidazolylthio Functionalized Resins

Masivuye M. Mahleba *, Jean-Luc Mukaba * and Zenixole R. Tshentu *

Department of Chemistry, Nelson Mandela University, P.O. Box 77000, Gqeberha 6031, South Africa Nelson Mandela University

* Correspondence: s212415204@mandela.ac.za (M.M.M.); s225198037@mandela.ac.za (J-L.M.); zenixole.tshentu@mandela.ac.za (Z.R.T.)

Abstract: Adsorbents derived from Merrifield's resin and a reaction with three functionalizing ligands namely 1,2-ethanedithiol (M-EDT), 1,2-benzenedithiol (M-BDT), and 2-benzimidazolylmethylthio acetic acid (M-BITAA), respectively, were synthesized for the recovery and separation of PGMs from simulated solutions. M-EDT, M-BDT and M-BITAA resins were characterized by FTIR, UV-Vis, TGA, CHNS and SEM techniques which confirmed significant structural modifications in these resins. Batch adsorption study revealed that M-BITAA exhibited the highest capacity for Pd(II) with about 26 $mg.g^{-1}$ while M-EDT and M-BDT resins were both below 10 $mg.g^{-1}$. The adsorbents obeyed the Langmuir isotherm in 0.8 M HCl solution. Batch adsorption further showed, in a competitive study, that M-BITAA was not selective for Pd(II) but an attractive sorbent for other PGMs such as Pt(IV) which may be advantageous for solutions containing these PGMs.

Keywords: platinum group metals; functionalized Merrifield's resin; adsorption studies

1. Introduction

The increasing demand for platinum group metals coupled with their limited availability in nature, has made their recovery a priority, especially considering the high cost of mining and refining [1]. Efficient and cost-effective methods of recovery from secondary sources such as spent catalytic converters, electronic waste and industrial by-products are needed [2,3]. Traditional recovery techniques, such as solvent extraction, precipitation, and electrochemical techniques, often fail to provide sufficient selectivity, leading to poor recovery rates or loss of other valuable metals. Furthermore, these methods can be environmentally damaging due to the use of toxic chemicals and the high energy costs associated with the processes [4]. Therefore, the need for more sustainable and efficient recovery technologies is evident. Recent research has highlighted the potential of adsorption-based techniques using functionalized resins [5]. These resins, when modified with specific functional groups, can selectively bind PGMs while excluding other metals, making them ideal for the targeted extraction. One such resin is Merrifield resin, originally developed for peptide synthesis, but has proven to be an effective material for adsorption when functionalized [6,7]. The incorporation of various functional groups onto Merrifield resin has shown promises in improving the selectivity and efficiency in capturing heavy metal ions from acidic solution [8]. One study investigated the use of Merrifield resin to immobilize quercetin by functionalizing the resin with oxi-(alkyl)n-OH spacers containing 6, 7, and 10 methylene units. This resulted in three variants of quercetin-immobilized materials, which were tested for Pb(II) adsorption under dynamic conditions at pH 5. The optimal adsorption capacities ranged from 0.64 to 1.21 $mg{\cdot}g^{-1}$ [9]. In another application, Merrifield resin was modified with ethylenediamine, methylamine, and dimethylamine to form primary, secondary, and tertiary amine-functionalized resins, respectively. These were evaluated for SO_2 adsorption using a packed bed column in a temperature-controlled oven. SO_2 gas was introduced at 100 $mL{\cdot}min^{-1}$ at

 doi:10.20944/preprints202504.2633.v1

25°C, with nitrogen as the purging gas, and adsorption was monitored via the effluent stream using a gas analyzer. The tertiary amine-functionalized resin showed the best SO_2 removal, achieving 99% efficiency at 25°C, which declined to 78.95% at 75°C [10].

The use of functionalized Merrifield resin in PGMs recovery represents an innovative approach that can address many of the challenges faced by traditional recovery methods. Functionalization involves the modification of a substrate, such as a resin or polymer, with specific functional groups that enhance its ability to selectively bind target metal ions [11]. Various functional groups have been explored for their ability to selectively bind Pd(II) ions, with thiol, amine, and imidazole [12,13] groups being among the studied. These functional groups can form strong bonds with Pd(II) generally through their S, N or O atom centers on the molecular structure, enhancing the resin's ability to adsorb the metal from solution [14,15]. Studies have demonstrated the effectiveness of functionalized Merrifield resins in selectively adsorbing Pd(II) from complex mixtures of metals [16,17]. Some of these functionalized Merrifield resin adsorbents exhibit high adsorption capacities exceeding the average efficiencies for Pd recovery [16–19]. Furthermore, these resins can be regenerated and reused multiple times without significant loss of adsorption capacity, making them cost-effective and sustainable for large-scale applications. The development of these advanced functionalized adsorbents is a significant step forward in the field of PGMs recovery, offering a more efficient and environmentally friendly alternative to traditional methods. This study focuses above all on the functionalization of Merrifield resin with dithiols and benzimidazolylthio functional groups for improved recovery of Pd(II).

2. Materials and Methods

2.1. Materials

Specialized materials including Merrifield Resin (50–100 mesh,1% cross-linked, 2.5–4.0 mmol $Cl^-.g^{-1}$, Sigma-Aldrich), Pd(II) standard (1000±3 mg. L^{-1}, Teknolab), 1,2-benzenedithiol (≥ 96%, Sigma-Aldrich), 1,2-ethanedithiol (≥ 98%, Fluka analytical) and 2-(benzimidazolylmethylthio) acetic acid (Aldrich) were used as obtained from the storage or pre-conditioned accordingly. Millipore water was prepared and used at all water involving instances

2.2. Characterization of Materials

Fourier Transform Infrared spectroscopy (Bruker Tensor 27) equipped with an attenuated total reflectance (ATR) was used to analyse the molecular composition and structural bonding of pristine and functionalised resins between 4000–400 cm^{-1}. Scanning electron microscopy (SEM) was employed with a Joel SEM JSM IT100 operated at 10 kV or 20 kV at a 7 or a 16 mm working distance. To improve the conductivity, all samples were coated prior to imaging by sputter coating using Gold. The diameter of the materials was measured from micrographs with ImageJ software. Thermogravimetric analysis (TGA, SDT Q600) was measured by heating the samples at a rate of 10°C.min^{-1} from 100–650°C. The data obtained was analyzed through a TA instrument © analysis software. UV-Vis spectra (Shimadzu UV-3100 spectrophotometer) was employed for detection of aromatic benzene and any other conjugated system and samples were scanned with photons in the range of 200–800 nm. The spectrometer was digitally operated using UV Probe 2.42 software. CHNS elemental analysis (carbon, hydrogen, nitrogen and sulfur) was performed on a Thermofisher Scientific organic (Elemental analyzer Flash 2000) after calibration with Cysteine, BBOT, Methionine and Sulfanilamide standards. The elemental composition of metal ions was carried out on a Perkin Elmer Avio 200 Inductively Coupled Plasma - Optical Emission Spectrometer (ICP-OES).

2.3. Synthesis Methods

2.3.1. Functionalization of Merrifield Resin with 1 ,2-Ethanedithiol and 1,2-Benzenedithiol

The functionalized Merrifield resin, M-BDT (using 180.18 mg of resin) and M-EDT (using 358.44 mg of resin) were respectively obtained using 1 mmol (84 μL) of 1 ,2-ethanedithiol (EDT) or 0.51 mmol

 doi:10.20944/preprints202504.2633.v1

(72 mg) of 1,2-benzenedithiol (BDT) in suitable amounts of triethyl amine (TEA) under refluxing at 60 °C for 12 hrs. The resulting solid was then filtered and extensively washed with tetrahydrofuran (THF), tetrahydrofuran-water (THF–H_2O) (1:1) mixture, H_2O, acetone, toluene, and acetone prior to characterization. When functionalizing the resin with EDT or BDT dimethylformamide (DMF) was used as the solvent, which is a polar aprotic solvent that can effectively dissolve both the dithiols and facilitate the nucleophilic substitution. TEA was employed in assistive amounts to deprotonate the dithiol, enhancing its nucleophilicity for substitution reactions with the benzyl chloride groups on the resin. This combination of solvent and base ensures effective functionalization of the resin, forming thiol-based functional groups on the polymer.

2.3.2. Functionalization of Merrifield Resin with 2-Benzimidazolylthio Acetic Acid

The functionalization of Merrifield resin with 2-benzimidazolylthio acetic acid (BITAA) was carried out using an esterification method modified from Matsumoto et al., (2014) [20]. 348.66 mg of Merrifield resin was swelled by suspension in THF overnight, while about 1 mmol (206.58 mg) of BITAA was weighed and mixed with equimolar amount of potassium carbonate (K_2CO_3) and tetrabutylammonium iodide ($N(n\text{-}Bu)_4I$), and the mixture was stirred at 90 °C until dissolved and colorless in THF. The resulting solution was then introduced to the swelled resin suspension and refluxed at 60 °C for 12 hrs. After the esterification, the brown solid was filtered and extensively washed with THF, H_2O–THF (1:1) mixture, H_2O, acetone, toluene, acetone, and then dried prior to characterization.

The schematic for functionalization of Merrifield resin with EDT, BDT and BITAA ligands and proposed chelating bidental for the complexes are shown in Figure 1. Disparities in adsorption ability are anticipated due to differences in the ligand environment and steric effects. M-BITAA, with its bulkier benzimidazolyl group, may form stronger complexes due to pi back bonding but with limited accessibility to metal ions. M-BDT and M-EDT feature thiol groups, with M-BDT having more steric hindrance due to its aromatic structure, while M-EDT is more flexible. The structural variations of these resins influence the stability, accessibility, and efficiency of metal ions.

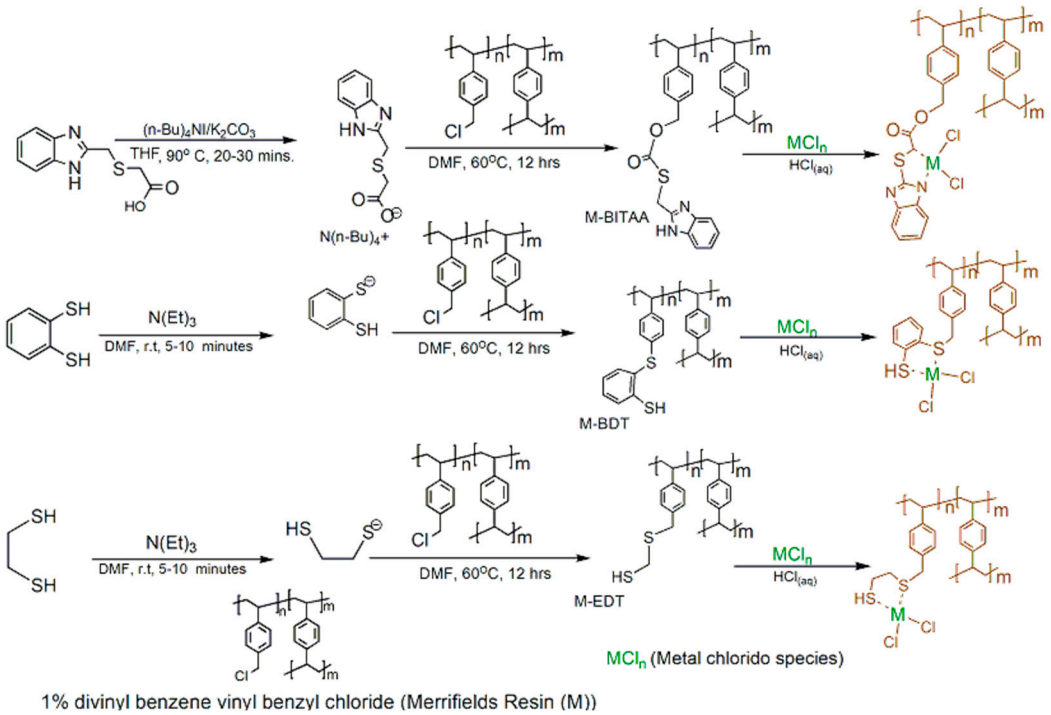

Figure 1. Schematic for functionalization of Merrifield resins with EDT, BDT and BITAA ligands (black) and bidentate chelation to palladium(II) (red).

 doi:10.20944/preprints202504.2633.v1

2.3.3. Adsorption Studies

Batch experiments were conducted at a fixed adsorbent dosage of 10 mg adsorbent per 10 ml adsorbate solution at varying HCl concentrations (0.01–1.5 M) with 5 mg.L^{-1} of Pd(II) solution to optimize the adsorbate acidity and Pseudo-first order (PFO) kinetics, pseudo-second order (PSO) kinetics, the Elovich equation, and intra-particle diffusion (IPD) are fundamental models used to describe various chemical reaction mechanisms; hence, they were the functions used to fit the obtained data. PFO kinetics is applicable when one reactant's concentration significantly exceeds that of the other, leading to a rate equation of the form equation 1, which, when linearized through integration with the natural logarithm, gives equation 2.

$$q_t = q_e\,(1-e^{(-k_1\,t)}) \tag{1}$$

$$\ln\,(q_e-q_t) = \ln q_e - k_1 t \tag{2}$$

where q_t and q_e (both in mg.g^{-1}) are values of the amount adsorbed at any given time of the process and the amount adsorbed at equilibrium, respectively and they can experimentally be established from concentration data via the equation (eq. 5 from t= 0—equilibrium). The value k_1 is the PFO rate constant. The values qe and k_1 according to the linear model can be achieved through a plot of ln(q_e-q_t) on the y-axis against time on the x-axis, and the y-intercept of the resulting straight line is the value ln q_e and the slope of the negative value of k_1. PSO kinetics, however, is often observed in systems where adsorption or multiple reactants are involved. The linearized form of this model is equation (Eq. 3).

$$\frac{t}{q_t} = \frac{1}{k_2\,q_e^2} + \frac{t}{q_e} \tag{3}$$

where q values are the same as explained for PFO and k_2 is the PSO rate constant.

The value h is defined by the denominator of the y-intercept ($h = k_2 q_e^2$) and defines the initial rate of adsorption in mg. g^{-1} .min^{-1}. while adsorption capacity of functionalized resins was determined between 5–150 mg.L^{-1} $[Pd(II)]_o$.

The above-mentioned adsorption capacity (mg.g^{-1}) and percent adsorption (adsorption efficiency) (q_t and E%) were calculated according to the equations (eq.4 and 5). Isothermal modelling studies were performed using Langmuir, Freundlich and Temkin models using their respective equations (eq. 6,7 and 8). $[Pd(II)]_0$ and $[Pd(II)]_e$ (mg.L^{-1}) also represented as C_e for isotherm models, denote the concentration of adsorbate ion Pd(II) before adsorption has taken place, and at the end when adsorption equilibrium has been reached, respectively. V and W denote the volume of adsorbate solution (ml) and the mass of adsorbent (mg) respectively. For isotherm model q_{max} (mg.g^1) denotes the adsorbent's maximum adsorption capacity, q_e (mg.g^{-1}) is the amount of target metal ion adsorbed onto adsorbent at equilibrium, K_L is the Langmuir coefficient (L.mg^1). K_F is a constant related to the adsorption capacity called the Freundlich coefficient, while n is another constant associated with the intensity of adsorption, known as the Freundlich constant. While the variables of the Temkin isotherm include K_T which denotes the Temkin equilibrium binding coefficient, b which denotes the Temkin constant, R the gas constant and T the system temperature. The influence of temperature was investigated at 25, 35, 45, 55, and 65 °C and the thermodynamic analysis was determined using the Van't Hoff equation (eq. 9) along with the Gibbs free energy equation (eq. 10). In the thermodynamic studies, the Van't Hoff equation consists of the variables including K_{eq} the dimensionless equilibrium constant, enthalpy (ΔH) and entropy (ΔS), while the Gibbs free energy also consists of the variable free energy (ΔG).

$$E\% = \frac{[Pd(II)]_o - [Pd(II)]_e}{[Pd(II)]_o} * 100\,\% \tag{4}$$

$$q_e = \frac{[Pd(II)]_o - [Pd(II)]_e}{W} * V \tag{5}$$

 doi:10.20944/preprints202504.2633.v1

$$q_e = \frac{q_{max} K_L C_e}{1 + K_L C_e} \quad (6)$$

$$q_e = K_F C_e^{(\frac{1}{n})} \quad (7)$$

$$q_e = \frac{RT}{b} \ln(K_T C_e) \quad (8)$$

$$\ln K_{eq} = -\frac{\Delta H}{RT} + \frac{\Delta S}{R} \quad (9)$$

$$\Delta G = \Delta H - T\Delta S \quad (10)$$

2.3.4. Competitive Study

Adsorption studies for PGMs competition were performed using solutions containing Pd(II), Pt(IV), and Ir(III) ions to assess the selectivity of resins. The adsorption was carried out in solutions containing different concentration ratios of metal ions (Pd: Pt: Ir at 1:1:1; 2:1:1 and 1:2:2 respectively labelled mixture 1, 2 and 3). Table 1 contains details of how the metal mixtures were prepared. These experiments were carried out at room temperature, 60 min, 150 rpm and optimum [Cl^-] (0.8 M) using 10 mg of resin in 10 mL of metal ion solution. The dimensionless selectivity factor (R) of the adsorbent towards metal ions was calculated as the quotient of adsorption capacity and that of the co-existing metal as shown in equation (eq. 11) where q_M and $q_{competing\ metal}$ (both in $mg.g^{-1}$) are the adsorption capacity values of the target metal ion and the competing metal ions respectively. R is reported for a target metal with respect to a specic competing metal in the same solution (R_{wrt} Competing Metal)

Table 1. The concentrations ($mg.L^{-1}$) of each of the tested metals initially available in solution in the three competitive scenarios considered by the current study.

	Pd ($mg.L^{-1}$)	Pt ($mg.L^{-1}$)	Ir ($mg.L^{-1}$)
Mixture 1	5	5	5
Mixture 2	10	5	5
Mixture 3	5	10	10

$$\boldsymbol{R_{wrt} Competing\ Metal = \frac{q_M}{q_{competing\ metal}}} \quad (11)$$

3. Results

3.1. Characterization of Materials

Figure 2(a) shows the IR spectrum of pristine Merrifield (M) and functionalized Merrifield (M-BDT, M-EDT and M-BITAA) resins. The strong peak at about 684 cm^{-1} was attributed to $\boldsymbol{\nu}$ (Benzyl-Cl) while the peak at 770 cm^{-1} is likely due of out-of-plane C-H bending vibrations of the benzene ring. This region is characteristic of aromatic substitutions, and its presence suggests that the benzyl structure remains intact after functionalization. These observations were consistent with peaks reported by Majavu et al. (2017) [21] and Dardouri et al. (2015) [22]. The peak located at 1268 cm^{-1} is characteristic for M resins and was attributed to CH_2-Cl bending. This peak exhibited reduced intensities in M-BDT, M-EDT and M-BITAA functionalized resins than pristine M resin. The decreased intensity of this peak might indicate a decrease in the CH_2-Cl population. Furthermore, all the resins displayed characteristic peaks at 1591, 1533, 1462, 2999, 2885, and 2883 cm^{-1} consistent with benzene ring vibrations and -CH stretches, aligning with findings from Liu et al. (2010) [23] and Boruah et al. (2013) [24]. The mentioned characteristic vibrations appear slightly shifted towards high

 doi:10.20944/preprints202504.2633.v1

wavenumbers (1600–1200 cm^{-1}) or low wavenumbers (3000–2800 cm^{-1}). The appearance of wavenumber shifting between unfunctionalized Merrifield resin and a derivative has been previously reported by Chen. (2007) [25]. The slight extent of these shifts could be indicative of preservation of the bulk polymer structure after functionalization. Furthermore, these shifts in M-BITAA could possibly be due to the introduction of S-, N- or O-bearing functionalities causing an electron withdrawing effect on the aromatic ring associated with these materials, and consequently its bond-shortening or stiffening and arising conjugation differences as they were pointed out for benzene ring vibrations [26]. Similarly to MBITAA, shifts observed in MBDT and MEDT could be due to reduction of -C-Cl bonds relative to -CH bonds and Cl substitution by N and S after the functionalization. Figure 2(b) shows the UV-Vis spectra of pristine stacked alongside functionalised resins. These results revealed notable shifts in electronic features. The unmodified M resin exhibited an absorption peak at 279 nm, corresponding to the polystyrene structure and aromatic groups [27,28]. Similarly to IR results, slight shifts were observed in the functionalized resins (M-BDT, M-EDT, and M-BITAA), suggesting changes in the electronic environment, more so for the dithiols where there are relatively higher absorbance values than for M-BITAA and the pristine resin. These shifts are consistent with previous studies [23,24]. The functionalization led to increased electronic conjugation, confirming successful modification of the resin surface. The thermal stability of the materials as shown in Figure 2(c) further revealed distinct degradation for pristine and functionalised resins. Pristine M resin showed a two-step degradation process at 237 °C and 400 °C with respective weight loss of 15% and 60%, and this was found to be comparable to the TGA pattern observed by Pisk et al. (2019) [27] whereby such weight loss pattern was attributed to the decomposition of Merrifield resin bulk structure. Similarly to the pristine resin, the decomposition of functionalised M-BITAA also largely occurred as a multistep process at 50, 245 and 420 °C corresponding to weight loss of 1.90, 15.56 and 55 % respectively. This is also associated to decomposition of the bulk structure of Merrifield resin [26]. In contrast to pristine M and M-BITAA resins, the functionalized M-EDT and M-BDT decomposed mainly at 63 (0.62%), 263 (7.21%), 313 (7.08%) and 400 °C (48.24%) for M-EDT, and 180 (5.35%), 275 (5.96%), 390 (54.84%), and 545 °C (9.54%) for M-BDT were respectively recorded for these resins.

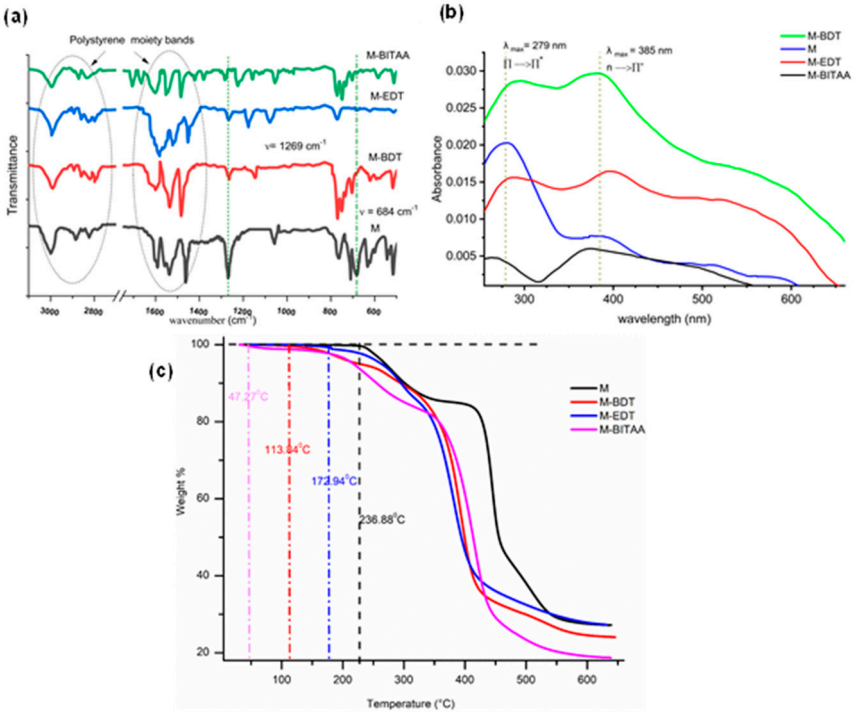

Figure 2. Depicts the (a) FTIR spectrum, (b) UV-Vis spectrum, and (c) TGA results of unfunctionalized (M) and functionalized (M-BDT, M-EDT and M-BITAA) resin materials.

 doi:10.20944/preprints202504.2633.v1

On the overall, the maximum degradation temperature was highest for the pristine M resin that its functionalized derivatives, contrasting with the findings of Boruah & Das (2018) [28] who studied Schiff base-functionalized resins. This discrepancy highlighted that sometimes the Merrifield resin becomes a little resistant to thermal degradation after functionalization while it may also become less thermally resilient sometimes as function of factors like functionalisation conditions such as solvent, temperature and functionalising agent's concentration [29,30]. The differences in decomposition events emphasize the effects of functionalization on the resin's thermal stability [31].

Figure 3 shows the SEM images of pristine M and functionalized M-BDT, M-EDT and M-BITAA resins. These micrographs revealed that the smoothness of the pristine M resin outer surface was altered indicating the effect of functionalization process. In contrast, the functionalized M-EDT, M-BDT and M-BITAA resins exhibited minor surface agglomerations which were finer in M-BITAA and coarser for M-EDT resins as also reported for dendrimer functionalised Merrifield resins [32,33]. The occurrence of functionalizing agent on the surface of Merrifield resin beads was attributed to solvent effect, reaction conditions or ligand reactivity [34–36]. The results further revealed that, the functionalisation of pristine M had a direct impact on its diameter depending on the additive. In fact, it was found that M-BITAA functionalisation increased the diameter of pristine M (211.2 μm) while M-EDT and M-BDT tended to decrease it. The diameters of the functionalised resins were respectively 193 μm, 207 μm and 224 μm for M-BDT, M-EDT and M-BITAA. These changes in diameter of resins align with findings from Lapinte et al. (2007) [37] and Kappert et al. (2019) [38], who attributed size variations to solvent effects and ligand properties. The observed effects are consistent with other studies on functionalized resins [39].

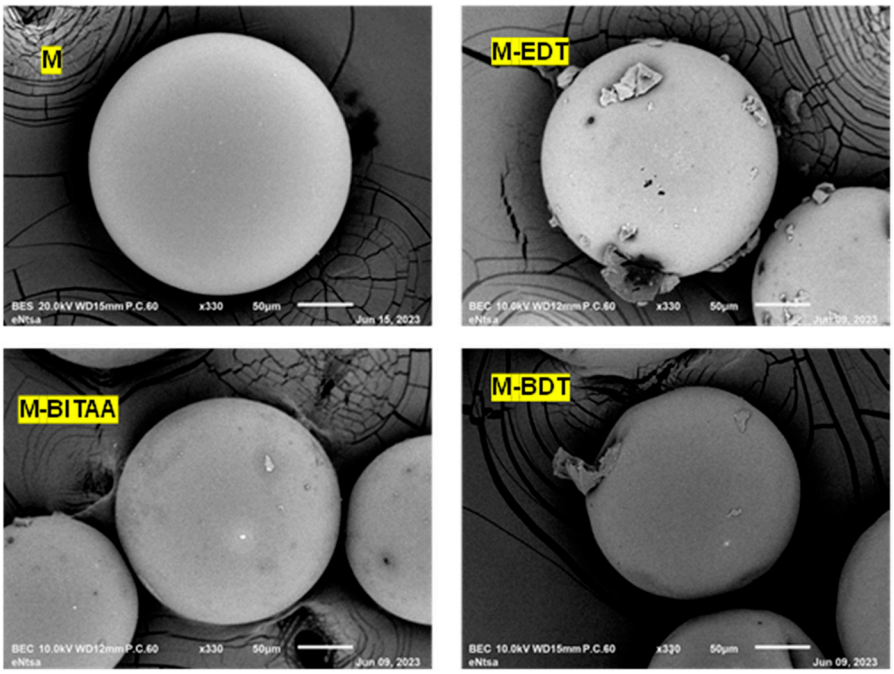

Figure 3. SEM micrographs of unfunctionalized (M) and functionalized (M-BDT, M-EDT and M-BITAA) resin materials.

CHNS analysis for elemental composition of resin before and after the functionalization was also carried out to support the SEM results. As can be seen in Table 2, it was found that pristine M resin contains carbon (79.00%), hydrogen (7.00%) and nitrogen (0.50%) with no sulfur. The degree of functionalization varied notably among the modified resins. M-EDT and M-BDT exhibited poor functionalization, as reflected in their very low sulfur content (0.03% and 0.01%, respectively). This indicates that the incorporation of dithiol groups was limited, leading to reduced sulfur percentages and lower functionalization efficiency (30–40% for M-EDT and only 5–8% for M-BDT). In contrast, M-BITAA demonstrated a significantly higher degree of functionalization, as indicated by its substantial

 doi:10.20944/preprints202504.2633.v1

increase in nitrogen content (4.00%) and the highest functionalization percentage (50–80%). This suggests a more successful incorporation of benzimidazolyl functional groups. The observed changes in carbon and hydrogen percentages further support these trends, with M-BITAA showing the most pronounced variations due to the additional functional groups introduced. M-BITAA exhibited a significant decrease in carbon (76.47%), an increase in hydrogen (7.44%), and nitrogen (4.46%), with sulfur at 0.040%. These changes are consistent with the functionalization processes, where specific ligands alter the resin's elemental composition, as suggested in literature [40].

Table 2. The elemental analysis of the pristine resin resins with a loading capacity of 2.5-4.0 mmol $Cl^{-}.g^{-1}$ and the functionalized resins.

Resins	C	H	N	S	% Functionalization
M (Pristine)	79.00	5.00	0.50	0.00	N/A
M-EDT	79.00	6.00	0.70	0.03	30-40
M-BDT	78.00	6.00	0.80	0.01	5-8
M-BITAA	76.00	7.00	4.00	0.04	50-80

3.2. Adsorption Studies

Figure 4 shows the results obtained at various acidic conditions and contact time using M-BITAA absorbent which had high degree of functionalization as previously discussed. It was observed that the shortest time to reach equilibrium and the maximum E% at each [HCl] value were in the order 0.01 M < 0.05 M < 0.1 M <1.5 M < 0.8 M ≈ 0.5 M. The data trend could be best fitted with polynomial functions of power 3—5. Therefore, kinetic studies were carried out under these conditions and the results of data fitting into four kinetic models for M-BITAA, M-BDT, and M-EDT are respectively shown in Figures S2, Figure S3 and Figure S4 while Table S1 summarizes the key parameters obtained from these fitting models. It was found that M-BITAA adsorbent best fitted Elovich, IPD and PSO with R^2 over 0.9 while M-EDT and M-BDT adsorbents best obeyed the PSO model with R^2 value over 0.9. Figure 6(a-b) shows the effect of initial Pd(II) concentration on adsorption efficiency (E%) and capacity (q_e) for functionalized M-BDT, M-EDT, and M-BITAA resins. As the Pd(II) concentration increased, the adsorption efficiency decreased, likely due to saturation of active sites on the adsorbents [41]. Conversely, adsorption capacity increases with concentration, reflecting a greater uptake of Pd(II) at higher concentrations [42]. Among the adsorbents, M-BITAA exhibits superior performance, achieving the highest q_e values. The observed trends highlight the trade-off between efficiency and capacity in adsorption processes [43]. M-BITAA being of a significantly higher Q_{max} (>25 $mg.g^{-1}$), reflects strong chelation via N- and S-centers [44–46] . The adsorption capacities for Pd(II) follow the order M-BITAA > M-EDT > M-BDT, which corresponds to the ligand loading percentages (Table 2).

 doi:10.20944/preprints202504.2633.v1

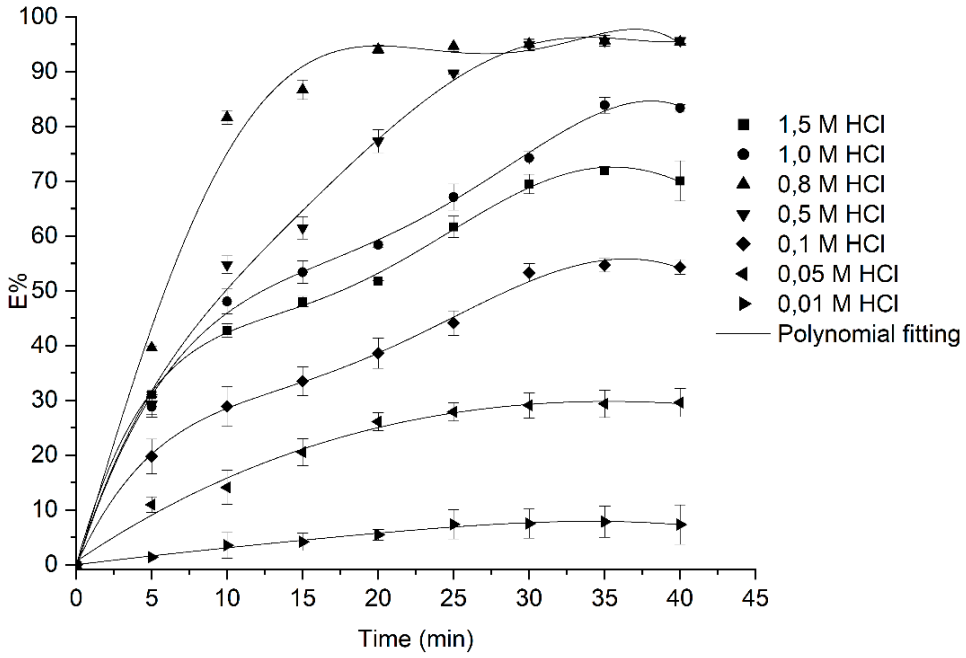

Figure 4. Adsorption percentage of M-BITAA across 40 minutes at [HCl] 1.5, 1.0, 0.8, 05, 0.1, 0.05, and 0.01 M.

The M-BITAA moiety features N,S coordination sites [47,48] and pi backbonding character, significantly boosting its adsorption capacity. M-EDT and M-BDT, with two S atoms, can form bidentate complexes and the lesser performing 1,2-benzenedithiol might be due to the rigid aromatic structure restricting its ability to form efficient chelate complexes [49,50] or simply attributed to the lower degree of functionalization. Overall, M-BITAA's higher ligand loading, versatile coordination modes, and favourable electronic structure make it the most efficient Pd(II) adsorbent. The optimum $[Pd(II)]_o$ for each adsorbent can be approximated based on the adsorption capacity trends in Figure 5(a-b). For M-BDT, q_e begins to plateau in the range of 55–60 $mg.L^{-1}$, suggesting this as the optimum concentration. M-EDT shows a similar trend, with q_e also levelling off around 55–60 $mg.L^{-1}$. In contrast, M-BITAA exhibits increasing q_e with a plateau starting much later from around 95–100 $mg.L^{-1}$, indicating that its optimum concentration is the nearest to the maximum tested value. These results highlight the differing performance and capacities of the adsorbents. This experimental data was then fitted into selected isothermal models to obtain mechanistic indications of the adsorption activity, and the results are shown in Figure 6. The results revealed that Langmuir isotherm model compliance occurred for all the adsorbents than other tested models. Thus, it could be posited that all the adsorbents exhibited monolayer adsorption of the adsorbate indicating likelihood that chemisorption is the type of interaction between adsorbate and adsorbent surface [51].

 doi:10.20944/preprints202504.2633.v1

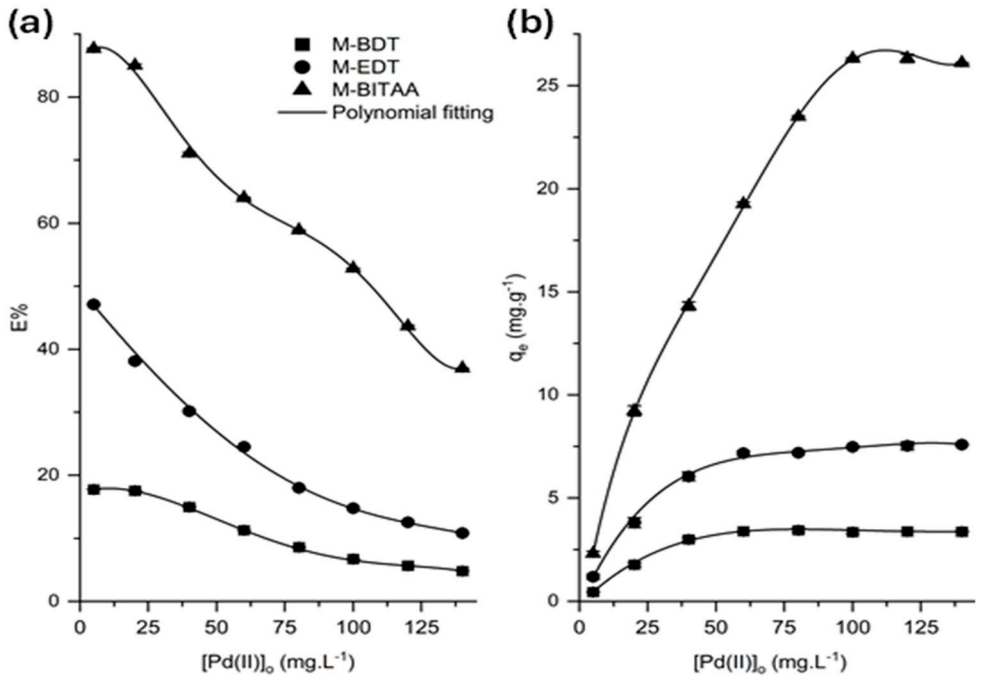

Figure 5. Pd(II) adsorption efficiency (a) and capacity (b) on M-EDT, M-BDT and M-BITAA modified resins in 0.8 M solution of HCl across 40 min.

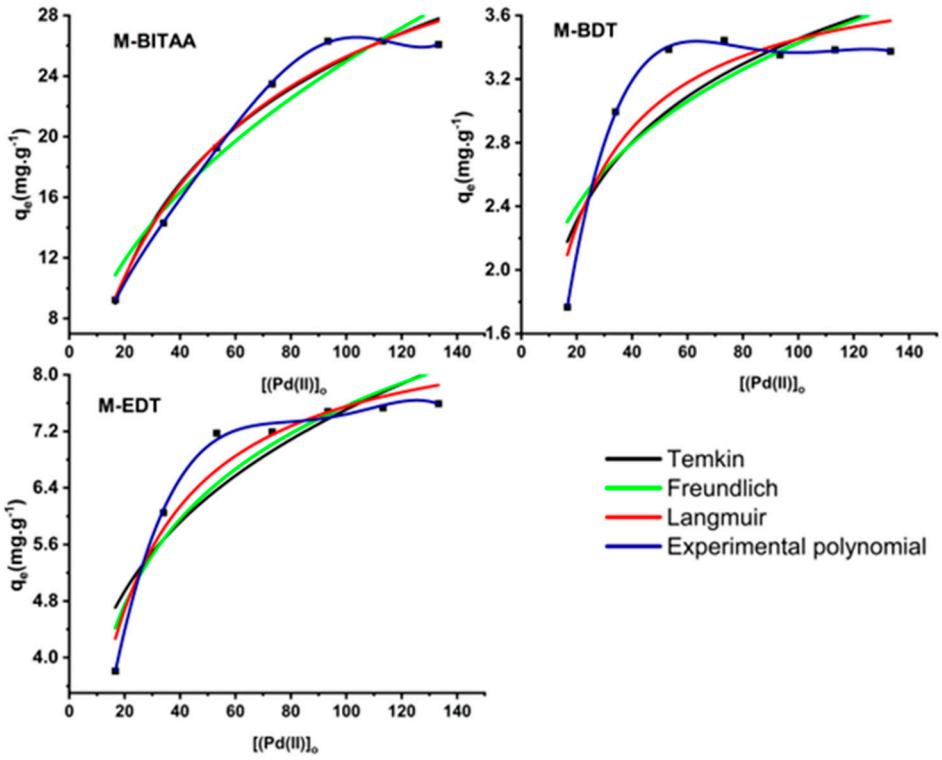

Figure 6. Experimental and non-linear isotherms of M-BITAA, M-BDT, and M-EDT resins.

Figure 7 shows the effect of temperature on the adsorption capacity of functionalized M-EDT, M-BDT and M-BITAA resins across 60 min. These results indicated that q_e values of all the modified resins increased with increasing contact time and were higher at lowest temperatures (room temperature). The evolution of q_e with time conformed with a cubic polynomial function and all the modified resins exhibited exothermic interaction with Pd(II) throughout both the contact time and temperature [52]. The data obtained was plotted according to the Van't Hoff equation Eq.9 and shown

 doi:10.20944/preprints202504.2633.v1

in Figure 8. It can be seen from this plot that all the materials exhibited positive slopes at all contact times where plateau were observed around 45 min. Then thermodynamic parameters were obtained from the data of the plots using the Gibbs free energy equation Eq.10 and are presented in Table S2. The enthalpy values were negative confirming exothermicity of process and were about 50 to 250 times the entropy values which implied that the process is enthalpy driven [53]. The Gibbs free energy (ΔG) values increased with temperature at all contact times until the 45th minute signifying a reduction in spontaneity with temperature increase, with the values of M-BITAA being comparable to the free energy levels associated with chemisorption [54]. M-BDT at the 15th minute had the highest ΔG values while M-BITAA at 45 minutes to the 60th minute had the smallest ΔG values thus these were respectively the situations and moments of the adsorption process where the least spontaneous and the most spontaneous adsorption happened. All the adsorbents displayed an increase in spontaneity with contact time increase. Subsequent to the above experiment, functionalized M-BITAA resin was selected and used for further study on the competition of Pd(II) with Pt(IV) and Ir(III). The obtained results are plotted in Figure 9 in terms of adsorption efficiency, and the established selectivity factors are presented in Table 3.

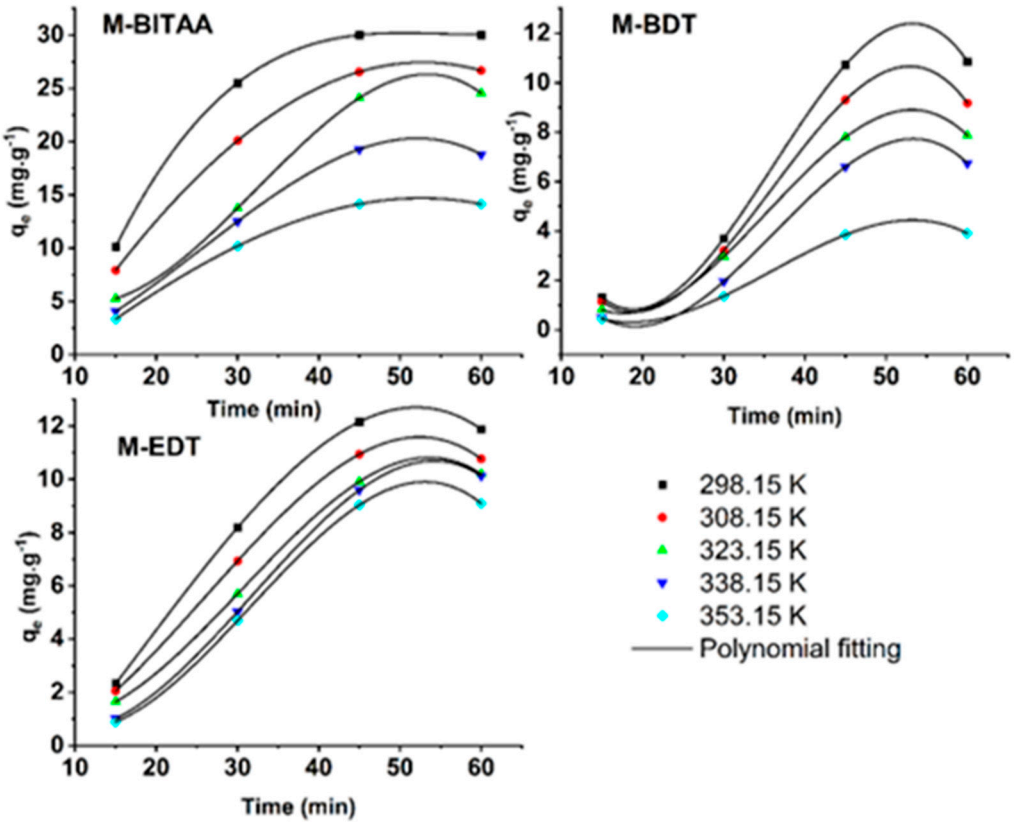

Figure 7. The effect of temperature across 60 min for M-BITAA, M-BDT and M-EDT resins.

Preprints.org (www.preprints.org) | NOT PEER-REVIEWED | Posted: 30 April 2025 doi:10.20944/preprints202504.2633.v1

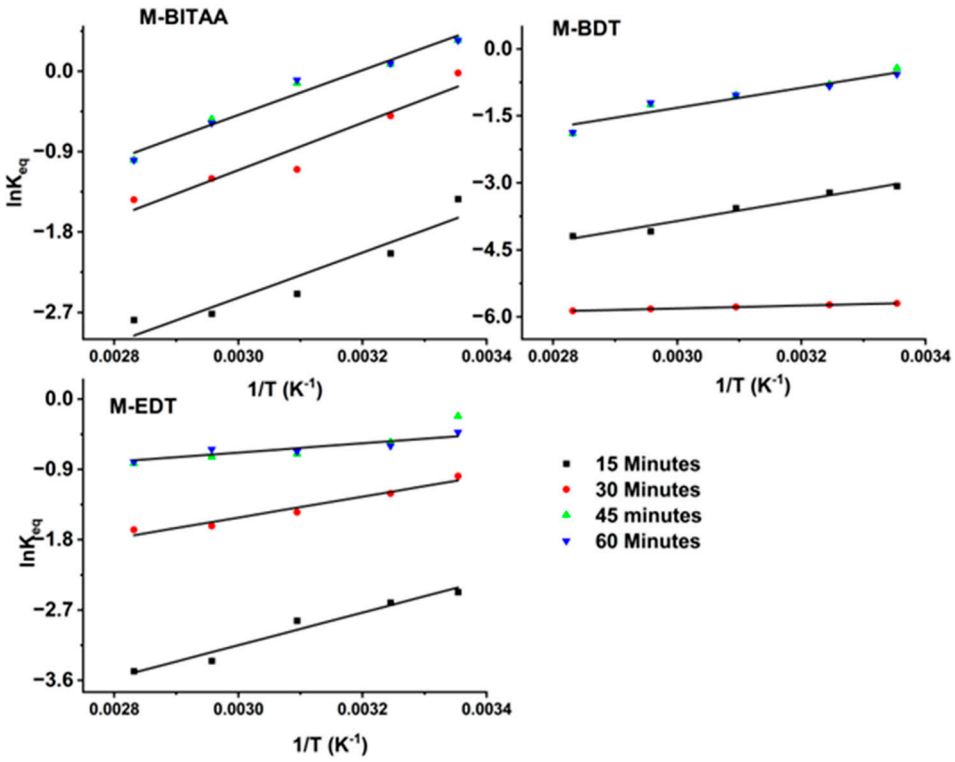

Figure 8. Van't Hoff plot for M-BITAA, M-BDT and M-EDT under varied contact time.

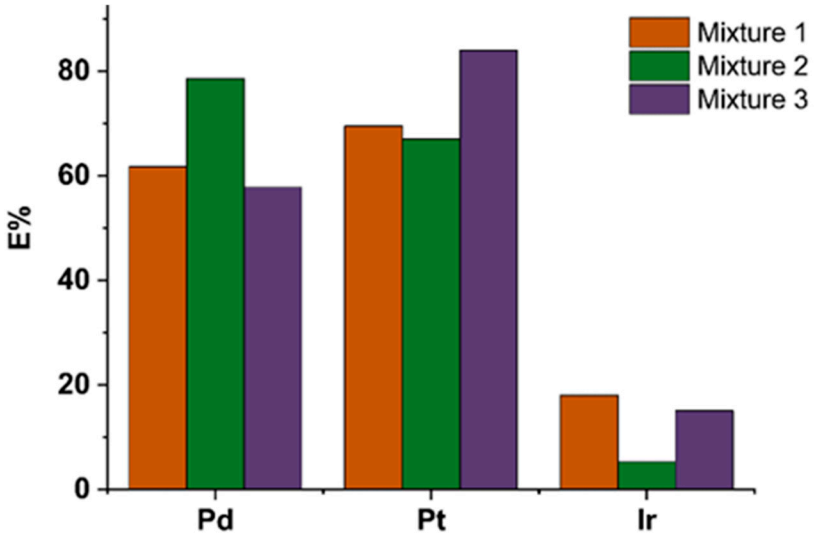

Figure 9. The adsorption efficiency of Pd(II), Pt(IV), and Ir(III) present at the same time in the adsorbate solution in three types of mixtures whereby their relative proportions were varied.

Table 3. The selectivity factors of M-BITAA towards Pd(II) in competition with Pt(IV) and Ir(III).

	R_{wrt} Pt (IV)	R_{wrt} Ir(III)
Mixture 1	0.81	3.58
Mixture 2	2.04	28.92
Mixture 3	0.32	1.91

M-BITAA demonstrated preferential adsorption for Pt(IV) over Pd(II) and Ir(III) with the selectivity factors of Pd(II) with respect to Pt(IV) (R_{wrt} Pt(IV) being 0.81, 2.04 and 0.32 respectively for mixture 1, 2 and 3 while R wrt Ir(III) values were 3.58, 28.92 and 1.91 respectively for the three

 doi:10.20944/preprints202504.2633.v1

different competition solutions mixture 1, 2 and 3. Given that mixture 1 consists of the Pt(IV) and the Ir(III) being present in equal concentration as Pd(II), while in mixture 2 they are half its concentration while in mixture 3 Pd(II) is twice the concentration of these two other competing metal species, the selectivity factors obtained highlighted the adsorbent's potential for simultaneous recovery of PGMs in complex mixtures [55–58] . This trend can be linked to the unique coordination environment provided by the benzimidazole moiety which is conducive to the hexacoordination typically required by Pt(IV).

4. Conclusion

This study investigated the adsorptive extraction of Pd(II)using Merrifield resin functionalized with dithiol (M-BDT, M-EDT) and benzimidazolyl-thioacetic acid (M-BITAA). The functionalization process was characterized by several techniques, including FTIR, UV-Vis, TGA, CHNS and SEM, which confirmed significant structural modifications in the resin. These modifications enhanced the adsorption performance of pristine Merrifield resins by introducing specific functional groups that improved metal ion binding. The optimal Pd(II) adsorption was achieved at 0.8 M HCl, with M-BITAA exhibiting the highest adsorption capacity due to its ability to chelate Pd(II) through N,S-chelation and even possible interaction through O centers. Adsorption efficiency was influenced by various factors such as Pd(II) initial concentration, contact time, and temperature, and all functionalized resins demonstrated exothermic adsorption behaviors. The adsorption data followed the Langmuir isotherm model indicating a chemisorption process, while thermodynamic studies revealed that the adsorption process was enthalpy-driven and exothermic. The study further assessed the selectivity of the resins, finding that M-BITAA showed less superior Pd(II) separation efficiency from Pt(IV) but more from Ir(III), while its potential for PGMs recovery was thus highlighted through its capability to absorb the PGMs making it a promising candidate for their simultaneous efficient recovery from aqueous acidic solutions.

Supplementary Materials: The following supporting information can be downloaded at the website of this paper posted on Preprints.org. **Figure S1.** M-BITAA linear fitting of kinetic models (a) PSO, (b) PFO, (c) Elovich, and (d) IPD; **Figure S2.** M-BDT linear fitting for kinetic models (a) PFO, (b) PSO, (c) Elovich, and (d) IPD; **Figure S3.** M-EDT fitted with kinetic models a) PFO, (b) PSO, (c) Elovich, and (d) IPD; **Table S1.** The parameters of kinetic performance and fitting of the obtained adsorption data of each adsorbent to the kinetic models considered for M-BITAA @ 0.5 M, and M-BDT and M-EDT @ 0.8 M. **Table S2**. Thermodynamic parameters obtained for M-BDT, M-EDT and M-BITAA at different times and over five different temperatures.

Funding: This research was funded by Nelson Mandela University and the National Research Foundation (grant number: CPRR230515106464).

Data Availability Statement: All the data related to this work is presented in this manuscript and in supplementary information.

Acknowledgments: The support of eNtsa and Stellenbosch Analytical Centre for analysis services is acknowledged. Mr. Henk Schalekamp for assistance with consumables and certain equipme..nt.

Conflicts of Interest: Authors declare no conflict of interest.

References

1. Hughes, A. E., Haque, N., Northey, S. A., & Giddey, S. (2021). Platinum group metals: A review of resources, production and usage with a focus on catalysts. Resources, 10(9), 93.
2. Gulliani, S., Volpe, M., Messineo, A., & Volpe, R. (2023). Recovery of metals and valuable chemicals from waste electric and electronic materials: a critical review of existing technologies. RSC Sustainability, 1(5), 1085-1108.

 doi:10.20944/preprints202504.2633.v1

3. Kaya, M. (2016). Recovery of metals and nonmetals from electronic waste by physical and chemical recycling processes. Waste Management, 100(57), 64-90.
4. Krishnan, S., Zulkapli, N. S., Kamyab, H., Taib, S. M., Din, M. F. B. M., Abd Majid, Z.,Chaiprapat, S., Kenzo, I., Ichikawa, Y., Nasrullah, M., Chelliapan,S., & Othman, N. (2021). Current technologies for recovery of metals from industrial wastes: An overview. Environmental Technology & Innovation, 22, 101525.
5. Lee, J. C., Hong, H. J., Chung, K. W., & Kim, S. (2020). Separation of platinum, palladium and rhodium from aqueous solutions using ion exchange resin: A review. Separation and Purification Technology, 246, 116896.
6. Siu, W. K. M. (2004). Applications and Microwave Assisted Synthesis of Poly (ethylene glycol) modified Merrifield resins.
7. Zviagin, I. M., Khimchenko, S. V., Blank, T. A., Shcherbakov, I. K., Bryleva, E. Y., Bunina, Z. Y., Sofronov, D,S., Belikov, K.N., & Chebanov, V. A. (2018). Merrifield resin-linked polyazole-based sorbent for heavy metal ions extraction from water. Functional Materials.
8. Fontenot, S. A., Carter, T. G., Johnson, D. W., Addleman, R. S., Warner, M. G., Yantasee, W., Warner, C.L., Fryxell, G,E.,& Bays, J. T. (2010). Nanostructured Materials for Selective Collection of Trace-Level Metals from Aqueous Systems. Trace Analysis with Nanomaterials, 191-221.
9. Fernández-Puig, S., Luaces-Alberto, M. D., Vallejo-Becerra, V., Teran, A. O., Chávez-Ramírez, A. U., & González, A. V. (2019). Modified Merrifield's resin materials used in capturing of Pb(II) ions in water. *Materials Research Express*, *6*(11), 115104.
10. Yu, X., Hao, J., Xi, Z., Liu, T., Lin, Y., & Xu, B. (2019). Investigation of low concentration SO_2 adsorption performance on different amine-modified Merrifield resins. *Atmospheric Pollution Research*, *10*(2), 404-411.
11. Pustam, A. N., & Alexandratos, S. D. (2010). Engineering selectivity into polymer-supported reagents for transition metal ion complex formation. Reactive and Functional Polymers, 70(8), 545-554.
12. Kang, T., Park, Y., & Yi, J. (2004). Highly selective adsorption of Pt^{2+} and Pd^{2+} using thiol-functionalized mesoporous silica. Industrial & Engineering Chemistry Research, 43(6), 1478-1484.
13. Liu, J. L., Sun, M., Shi, Y. H., Zhou, X. M., Zhang, P. Z., Jia, A. Q., & Zhang, Q. F. (2022). Functional modification, self-assembly and application of calix [4] resorcinarenes. Journal of Inclusion Phenomena and Macrocyclic Chemistry, 102(3), 201-233.
14. Tofan, L., & Wenkert, R. (2022). Chelating polymers with valuable sorption potential for development of precious metal recycling technologies. Reviews in Chemical Engineering, 38(2), 167-183.
15. Wu, F., Ye, G., Yi, R., Sun, T., Xu, C., & Chen, J. (2016). Novel polyazamacrocyclic receptor decorated core–shell superparamagnetic microspheres for selective binding and magnetic enrichment of palladium: synthesis, adsorptive behavior and coordination mechanism. Dalton transactions, 45(23), 9553-9564.
16. Fayemi, O. E., Ogunlaja, A. S., Kempgens, P. F., Antunes, E., Torto, N., Nyokong, T., & Tshentu, Z. R. (2013). Adsorption and separation of platinum and palladium by polyamine functionalized polystyrene-based beads and nanofibers. Minerals Engineering, 53, 256-265.
17. Kancharla, S., & Sasaki, K. (2023). Selective extraction of precious metals from simulated automotive catalyst waste and their conversion to carbon supported PdPt nanoparticle catalyst. Colloids and Surfaces A: Physicochemical and Engineering Aspects, 665, 131179.
18. Mildan, E., & Gülfen, M. (2015). Equilibrium, kinetics, and thermodynamics of Pd (II) adsorption onto poly (m-aminobenzoic acid) chelating polymer. Journal of Applied Polymer Science, 132(37).
19. Sari, A., Mendil, D., Tuzen, M., & Soylak, M. (2009). Biosorption of palladium (II) from aqueous solution by moss (Racomitrium lanuginosum) biomass: Equilibrium, kinetic and thermodynamic studies. Journal of Hazardous Materials, 162(2-3), 874-879.

 doi:10.20944/preprints202504.2633.v1

20. Matsumoto, K., Shimazaki, H., Miyamoto, Y., Shimada, K., Haga, F., Yamada, Y., Miyazawa, H., Nishiwaki, K,.& Kashimura, S. (2014). Simple and convenient synthesis of esters from carboxylic acids and alkyl halides using tetrabutylammonium fluoride. Journal of Oleo Science, 63(5), 539-544.
21. Majavu, A., Ogunlaja, A. S., & Tshentu, Z. R. (2017). Separation of rhodium(III) and iridium(IV) chlorido complexes using polymer microspheres functionalised with quaternary diammonium groups. Separation Science and Technology, 52(1), 71-80.
22. Dardouri, M., Ammari, F., & Meganem, F. (2015). Aminoalkylated Merrifield resins reticulated by tris-(2-chloroethyl) phosphate for cadmium, copper, and iron(II) extraction. International Journal of Polymer Science, 2015.
23. Liu, J., Li, P., Zhang, Y., Ren, K., Wang, L., & Wang, G. (2010). Recyclable Merrifield resin-supported organocatalysts containing pyrrolidine unit through A3-coupling reaction linkage for asymmetric Michael addition. Chirality, 22(4), 432-441
24. Boruah, J. J., Das, S. P., Ankireddy, S. R., Gogoi, S. R., & Islam, N. S. (2013). Merrifield resin supported peroxomolybdenum (VI) compounds: recoverable heterogeneous catalysts for the efficient, selective and mild oxidation of organic sulfides with H 2 O 2. Green chemistry, 15(10), 2944-2959.
25. Chen, G. (2007). Surface modification with polymers using living radical polymerisation and click chemistry (Doctoral dissertation, University of Warwick).
26. Kachhap, P., & Haldar, C. (2024). Catalytic Oxidation of Aliphatic Alcohols by Hydrogen Peroxide Using Merrifield Resin-Supported Binuclear Dioxidovanadium(v) Complexes of Hydrazone Ligands as a Catalyst. Topics in Catalysis, 1-21.
27. Pisk, J., Agustin, D., & Poli, R. (2019). Organic salts and Merrifield resin supported $[PM_{12}O_{40}]^{3-}$(M= Mo or W) as catalysts for adipic acid synthesis. Molecules, *24*(4), 783.
28. Boruah, J. J., & Das, S. P. (2018). Solventless, selective and catalytic oxidation of primary, secondary and benzylic alcohols by a Merrifield resin supported molybdenum(VI) complex with H_2O_2 as an oxidant. RSC advances, 8(60), 34491-34504.
29. Maurya, M. R., Chaudhary, N., & Avecilla, F. (2014). Polymer-grafted and neat vanadium(V) complexes as functional mimics of haloperoxidases. Polyhedron, 67, 436–448. doi:10.1016/j.poly.2013.09.021
30. Huang, Y. (2013). Novel applications of surface-modified sporopollenin exine capsules (Doctoral dissertation, University of Hull).
31. Edo, G. I., Ndudi, W., Ali, A. B., Yousif, E., Zainulabdeen, K., Onyibe, P. N., Ekokotu, H, A., Isoje, E.F.,Essaghah, A.E., Agmed, D.S., Umar, D.,& Ozsahin, D. U. (2024). Poly(vinyl chloride) (PVC): an updated review of its properties, polymerization, modification, recycling, and applications. Journal of Materials Science, 1-44.
32. Rajesh Krishnan, G., & Sreekumar, K. (2008). Catalysis by Polymer Supported Dendrimers, their Metal Complexes and Nanoparticle Conjugates (Doctoral dissertation, Cochin University of Science and Technology).
33. Dalla Valle, C. (2017). Novel mesoporous polymers and their application in heterogeneous catalysis (Doctoral thesis University of padua).
34. Lamblin, M., Nassar-Hardy, L., Hierso, J. C., Fouquet, E., & Felpin, F. X. (2010). Recyclable heterogeneous palladium catalysts in pure water: Sustainable developments in Suzuki, Heck, Sonogashira and Tsuji–Trost reactions. Advanced Synthesis & Catalysis, *352*(1), 33-79.
35. Barbey, R., Lavanant, L., Paripovic, D., Schuwer, N., Sugnaux, C., Tugulu, S., & Klok, H. A. (2009). Polymer brushes via surface-initiated controlled radical polymerization: synthesis, characterization, properties, and applications. Chemical Reviews, *109*(11), 5437-5527.

 doi:10.20944/preprints202504.2633.v1

36. Biernat, J. F., Konieczka, P., Tarbet, B. J., Bradshaw, J. S., & Izatt, R. M. (1994). Complexing and chelating agents immobilized on silica gel and related materials and their application for sorption of inorganic species. Separation and Purification Methods, *23*(2), 77-348.
37. Lapinte, V., Montembault, V., Houdayer, A., & Fontaine, L. (2007). Surface initiated ring-opening metathesis polymerization of norbornene onto Wang and Merrifield resins. Journal of Molecular Catalysis A: Chemical, 276(1-2), 219-225.
38. Kappert, E. J., Raaijmakers, M. J., Tempelman, K., Cuperus, F. P., Ogieglo, W., & Benes, N. E. (2019). Swelling of 9 polymers commonly employed for solvent-resistant nanofiltration membranes: A comprehensive dataset. Journal of Membrane Science, 569, 177-199.
39. Das, D., Sivaramakrishna, A., Brahmmananda Rao, C. V. S., Sivaraman, N., & Vijayakrishna, K. (2018). Phosphoramidate-functionalized Merrifield resin: synthesis and application in actinide separation. Polymer International, 67(4), 374-379.
40. Seyhan, S., Çolak, M., Merdivan, M., & Demirel, N. (2007). Solid phase extractive preconcentration of trace metals using p-tert-butylcalix [4] arene-1 , 2-crown-4-anchored chloromethylated polymeric resin beads. Analytica Chimica Acta, 584(2), 462-468.
41. Hossain, M. S., Hossain, M. S., Ahmed, S., & Mobarak, M. B. (2024). Characterization and adsorption performance of nano-hydroxyapatite synthesized from Conus litteratus waste seashells for Congo red dye removal. RSC Advances, 14(52), 38560-38577.
42. Ogata, F., Inoue, K., Tominaga, H., Iwata, Y., Ueda, A., Tanaka, Y., & Kawasaki, N. (2013). Adsorption of Pt(IV) and Pd(II) from aqueous solution by calcined gibbsite (Aluminum hydroxide). e-Journal of Surface Science and Nanotechnology, 11, 40-46.
43. Cao, M., Wang, J., Liu, X., Pei, Y., Gao, M., Wang, W., & Yang, H. (2023). Bio-inspired adsorbent with ultra-uniform and abundance sites accelerate breaking the trade-off effect between adsorption capacity and removal efficiency. Chemical Engineering Journal, 465, 142790.
44. Alias, M. F., Obed, S. M., & Jassim, A. H. (2007). Synthesis and characterization of the heavy metals; Au(III), Pd(II), Pt(IV) Rh(III) complexes of s–propynyl 2–thiobenzimidazole. Baghdad Science Journal, 4(1), 95-101.
45. Sharma, R. K., Kumar, H., & Kumar, A. (2015). A highly efficient and magnetically retrievable functionalized nano-adsorbent for ultrasonication assisted rapid and selective extraction of Pd^{2+} ions from water samples. RSC Advances, 5(54), 43371-43380.
46. Petrova, P., Chochkova, M., & Karadjov, M. (2022). Adsorption of Pd(II) on N- and S-modified silica sorbents. Journal of Chemical Technology & Metallurgy, 57(5).
47. Elsayed, S. A., Badr, H. E., di Biase, A., & El-Hendawy, A. M. (2021). Synthesis, characterization of ruthenium(II), nickel(II), palladium (II), and platinum (II) triphenylphosphine-based complexes bearing an ONS-donor chelating agent: Interaction with biomolecules, antioxidant, in vitro cytotoxic, apoptotic activity and cell cycle analysis. Journal of Inorganic Biochemistry, 223, 111549.
48. Kumar, S. B., Solanki, A., & Kundu, S. (2017). Copper(II) and palladium(II) complexes with tridentate NSO donor Schiff base ligand: Synthesis, characterization and structures. Journal of Molecular Structure, 1143, 163-167.
49. [45] Jiang, L., Liu, Y., Meng, X., Xian, M., & Xu, C. (2021). Adsorption behavior study and mechanism insights into novel isothiocyanate modified material towards Pd^{2+}. Separation and Purification Technology, 277, 119514.
50. Zhao, Y., Xu, C., Qi, Q., Qiu, J., Li, Z., Wang, H., & Wang, J. (2022). Tailoring delicate pore environment of 2D Covalent organic frameworks for selective palladium recovery. Chemical Engineering Journal, 446, 136823.

 doi:10.20944/preprints202504.2633.v1

51. Scheufele, F. B., Módenes, A. N., Borba, C. E., Ribeiro, C., Espinoza-Quiñones, F. R., Bergamasco, R., & Pereira, N. C. (2016). Monolayer–multilayer adsorption phenomenological model: Kinetics, equilibrium and thermodynamics. Chemical Engineering Journal, 284, 1328-1341.
52. Fujiwara, K., Ramesh, A., Maki, T., Hasegawa, H., & Ueda, K. (2007). Adsorption of platinum(IV), palladium(II) and gold(III) from aqueous solutions onto l-lysine modified crosslinked chitosan resin. Journal of Hazardous Materials, 146(1-2), 39-50.
53. Xu, L., Zhang, A., Zhang, F., & Liu, J. (2017). Preparation and characterization of a novel macroporous silica-bipyridine asymmetric multidentate functional adsorbent and its application for heavy metal palladium removal. Journal of hazardous materials, 337, 178-188.
54. Li, M., Wang, M., Zhang, L., Fan, Y., Xu, L., Ma, Z., Wen, Z., Wang, H., & Cheng, N. (2023). Adsorption of Pd(II) ions by electrospun fibers with effective adsorption sites constructed by N, O atoms with a particular spatial configuration: mechanism and practical applications. Journal of Hazardous Materials, 458, 132014.
55. Lin, S., Bediako, J. K., Cho, C. W., Song, M. H., Zhao, Y., Kim, J. A., Choi, J.W., & Yun, Y. S. (2018). Selective adsorption of Pd(II) over interfering metal ions (Co(II), Ni(II), Pt(IV)) from acidic aqueous phase by metal-organic frameworks. Chemical Engineering Journal, 345, 337-344.
56. Uheida, A., Iglesias, M., Fontàs, C., Hidalgo, M., Salvadó, V., Zhang, Y., & Muhammed, M. (2006). Sorption of palladium (II), rhodium (III), and platinum (IV) on Fe_3O_4 nanoparticles. Journal of colloid and interface science, 301(2), 402-408.
57. Fayemi, O. E., Ogunlaja, A. S., Antunes, E., Nyokong, T., & Tshentu, Z. R. (2015). The development of palladium (II)-Specific amine-functionalized silica-based microparticles: adsorption and column separation studies. Separation Science and Technology, 50(10), 1497-1506.
58. Moleko-Boyce, P., Makelane, H., Ngayeka, M. Z., & Tshentu, Z. R. (2022). Recovery of platinum group metals from leach solutions of spent catalytic converters using custom-made resins. Minerals, *12*(3), 361.